Evaluation of Lattice Light Shift at Low 10^{-19} Uncertainty for a Shallow Lattice Sr Optical Clock

Kyungtae Kim, Alexander Aeppli, Tobias Bothwell, and Jun Ye
JILA, National Institute of Standards and Technology and the University of Colorado, Boulder, Colorado 80309-0440, USA and Department of Physics, University of Colorado, Boulder, Colorado 80309-0390, USA

(Received 28 October 2022; accepted 23 February 2023; published 15 March 2023)

A Wannier-Stark optical lattice clock has demonstrated unprecedented measurement precision for optical atomic clocks. We present a systematic evaluation of the lattice light shift, a necessary next step for establishing this system as an accurate atomic clock. With precise control of the atomic motional states in the lattice, we report accurate measurements of the multipolar and the hyperpolar contributions and the operational lattice light shift with a fractional frequency uncertainty of 3.5×10^{-19}.

DOI: 10.1103/PhysRevLett.130.113203

Introduction.—Optical lattice clocks are advancing measurement precision to an unprecedented level [1,2]. Achieving a similar level of measurement accuracy is both an expected natural development and a necessary condition for the future redefinition of time [3–12].

The Sr optical lattice clock at JILA Sr1 employs a shallow one-dimensional (1D) optical lattice with enhanced atomic coherence and record low self-synchronous frequency instability [1]. This 1D lattice is established within an optical cavity oriented along the direction of gravity. Since neighboring sites are detuned by the gravitational potential energy difference, ultracold atoms confined in the lattice are described by Wannier-Stark (WS) wave functions [13]. Important ingredients for such significant progress in clock precision include cooling a large yet dilute sample of fermionic ^{87}Sr atoms to below 100 nK, well-characterized motional states, microscopic imaging spectroscopy, long atomic coherence time (> 30 s), and the precise control of atomic interaction effects. Further, at low lattice depths atom-atom interactions are modified, effectively eliminating density-dependent frequency shifts [14]. Thus, a shallow, partially delocalized, WS optical lattice clock contains ideal characteristics for next generation timekeeping.

While the spectroscopy lattice depth is far lower than previous clocks, the light shift associated with the lattice trapping light remains a key systematic. In this Letter, we report a detailed investigation of clock operation under engineered motional states within this titled lattice [Fig. 1(a)]. We provide a detailed study of lattice light shifts for lattice frequency, atomic motional states, and lattice depths near zero. In addition to reducing the total uncertainty of the lattice light shift down to 3.5×10^{-19} fractional frequency, we also report measurements of the light shift coefficients associated with the electric quadrupole ($E2$), magnetic dipole ($M1$) moments, and the hyperpolarizability.

Lattice light shift model.—Before we set out to perform systematic measurements of the lattice light shift, we take important steps to reduce systematic effects. The cavity-based lattice establishes a stable and well-defined light mode and intensity calibrated directly to the trap depth. The density related frequency shift is reduced and precisely measured to remove the atomic interaction effects when the lattice depth is varied. The motional state and related transverse temperature are monitored with an independent probe, which is important for measuring the contribution from the $E2$-$M1$ term.

The lattice light shift model is proposed for a lattice without considering the tunneling effect [16–18]. Since the gravitational tilt of the lattice is small compared to the band gap, the model is valid with WS states [19]. Here, we vary the lattice trap depth ranging from the WS regime to the more traditional isolated lattice configuration to explore the light shift effects.

The lattice light shift of the clock transition $\Delta\nu_{\mathrm{LS}}$ can be expressed as a function of three control parameters: the lattice depth u, lattice frequency ν_L, and the axial state quantum number n_z. Following the convention established in Refs. [16,17], the lattice light shift can be written as

$$\begin{aligned} h\Delta\nu_{\mathrm{LS}}(u,\delta_L,n_z) \approx & \left(\frac{\partial\tilde{\alpha}^{E1}}{\partial\nu}\delta_L - \tilde{\alpha}^{qm}\right)\left(n_z+\frac{1}{2}\right)u^{1/2} \\ & - \left[\frac{\partial\tilde{\alpha}^{E1}}{\partial\nu}\delta_L + \frac{3}{2}\tilde{\beta}\left(n_z^2+n_z+\frac{1}{2}\right)\right]u^1 \\ & + 2\tilde{\beta}\left(n_z+\frac{1}{2}\right)u^{3/2} - \tilde{\beta}u^2. \end{aligned} \tag{1}$$

The transverse motional effect is accounted for with the use of an effective depth, $u^j = (1 + jk_BT_r/u_0E_r)^{-1}u_0^j$, where k_B is the Boltzmann constant, T_r the radial temperature measured by transverse Doppler spectroscopy [Fig. 1(d)], $u_0 = U_0/E_r$ is the peak lattice depth, and the superscript j represents the thermally averaged jth power of the lattice

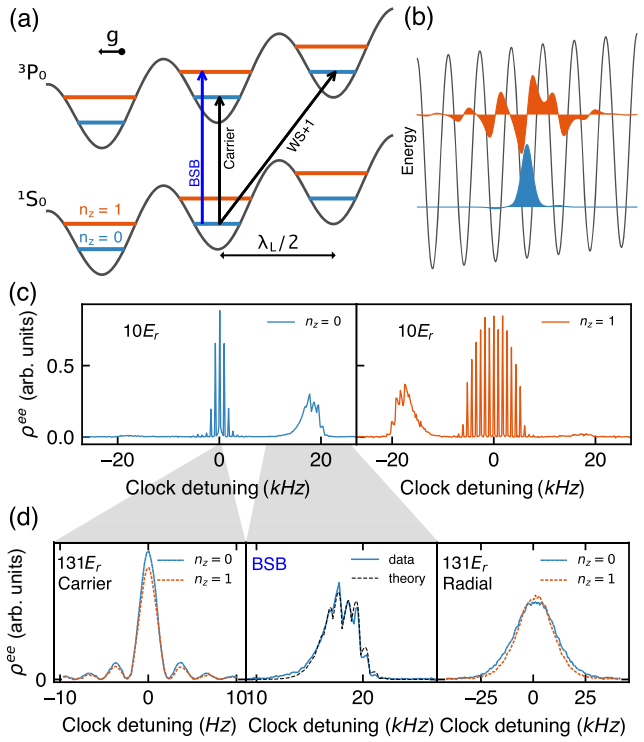

FIG. 1. (a) Schematics of the 1D optical lattice system. Gravity g lifts the energy degeneracy between adjacent lattice sites by $mg\lambda_L/2$. The clock carrier transition drives only $^1S_0 - {}^3P_0$ without changing the axial quantum number n_z and is used to probe lattice light shift. For the axial state control, we use the blue sideband (BSB) to drive $|n_z = 0\rangle$ to $|n_z = 1\rangle$. WS $\pm\, i$ denotes a transition to an i-site-shifted Wannier-Stark (WS) state. (b) Eigenstates of $n_z = 0$ (blue) and $n_z = 1$ (red) at $U_0 = 15E_r$. The offset of the wave function corresponds to eigenenergy of the lattice potential. (c),(d) Characterization of the motional states. (c) The left-hand (right-hand) panel shows the axial sideband spectrum of $|n_z = 0\rangle$ ($|n_z = 1\rangle$). ρ^{ee} is the excitation fraction. We adiabatically ramp U_0 to $10E_r$, which supports only two axial states. Sidebands close to the carrier are WS $\pm\, i$ transitions. (d) The left-hand panel shows Rabi spectra of the two axial states. In the middle, we enlarge the motional sideband and plot with the theoretical line shape [15] taking into account WS $\pm\, i$ sidebands. The right-hand panel shows the Doppler broadening to extract T_r. For $|n_z = 0\rangle$, T_r is 500 nK. For $|n_z = 1\rangle$, T_r is 40% lower, likely due to the limited transfer efficiency and reduced trapping potential.

depth [18]. $E_r = h^2/2m\lambda_L^2$, where m is the mass of ^{87}Sr and $\lambda_L = c/\nu_L$ the lattice wavelength, h is the Planck constant, with c the speed of light. $\delta_L = \nu_L - \nu^{E1}$ is the detuning from $E1$ magic frequency (ν^{E1}), including both the differential scalar shift and an experiment-specific differential tensor shift.

There are four dependent coefficients to be characterized, including ν^{E1}. $\partial\tilde{\alpha}^{E1}/\partial\nu$ is the frequency derivative of the differential electric dipole ($E1$) polarizability between $|^1S_0, m_F = \pm\frac{5}{2}\rangle$ and $|^3P_0, m_F = \pm\frac{3}{2}\rangle$ near ν^{E1}. This term includes both the scalar and tensor contributions, while the vector contribution is canceled by clock interrogation of opposite sign m_F states. $\tilde{\alpha}^{qm}/h$ is the differential multipolar polarizability in units of hertz, and $\tilde{\beta}/h$ is the differential hyperpolarizability in units of hertz. The variation of n_z is critical for enhancing the sensitivity to $\tilde{\alpha}^{qm}/h$, because different wave function extensions of $|n_z = 1\rangle$ and $|n_z = 0\rangle$ [Fig. 1(b)] vary the weighting factor between $E1$ (maximum at the lattice antinode) and $E2$-$M1$ (maximum at the node).

We systematically explore Eq. (1) by measuring the frequency difference between two control parameter sets. We vary the lattice depth from $3E_r$ to $300E_r$, δ_L over ± 200 MHz, and $n_z = 0$ and 1. When we modulate u and δ_L, the reference is chosen to be at the magic lattice depth to suppress the systematic error from collisional shifts [14]. We do not investigate the separation of tensor and scalar polarizability because they are integrated into $\partial\tilde{\alpha}^{E1}/\partial\nu$.

Clock in tilted, shallow lattice.—Our 1D ^{87}Sr optical lattice clock is detailed in previous publications [1,14]. We prepare stretched states ($m_F = \pm\frac{9}{2}$) spin-polarized ensembles in a single motional ground state axially and $T_r \sim 700$ nK radially at $U_0 = 300E_r$. The lattice intensity is adiabatically ramped to a range of depths and T_r is confirmed to vary from 700 to 60 nK. The atom number is about 10^5 for (u, ν_L) dependence measurement and 2×10^4 for n_z dependence measurement. Figure 1(c) presents a spectroscopic characterization of the motional state distribution of the atoms. After the preparation, we lower the lattice depth to the desired level and transfer the spin states with a series of clock π pulses together with cleaning pulses. In all cases, we use the magnetically insensitive $|^1S_0, m_F = \pm\frac{5}{2}\rangle \rightarrow |^3P_0, m_F = \pm\frac{3}{2}\rangle$ transition. For axial state control, a clock pulse resonant to the blue sideband [shown in Fig. 1(a)] drives $|n_z = 0\rangle \rightarrow |n_z = 1\rangle$ at $U_0 = 22E_r$. Transfer efficiency is about 15%–20% and results in a T_r reduction of 40% [see Fig. 1(d)]. Nevertheless, this temperature difference is negligible due to the low temperature and the proximity to the $E1$ magic frequency.

We use a cryogenic-silicon-cavity-stabilized laser to drive the clock transition [20,21]. Two interleaved atomic servos at two different conditions (u, δ_L, n_z) track the clock resonance and continuously average the differential frequency shift [22]. With a cavity stability of 4×10^{-17}, the Dick effect limited self-comparison stability is about 2×10^{-16} at 1 s with 380 ms Rabi pulse and about 1 s duty cycle. We determine the frequency shift by averaging collected frequency differences and assign 1σ statistical uncertainty from a fit to the overlapping Allan deviation taken at 1/3 of the total measurement time τ. In all cases, density shift corrected Allan deviations of the frequency difference follow the expected white frequency noise trend of $1/\sqrt{\tau}$. Typical uncertainties are less than 3×10^{-18} for (u, δ_L) modulation and about 5×10^{-18} for n_z modulation.

We apply a 70 μT bias magnetic field during the clock interrogation. The direction is parallel to the polarization of the lattice laser to minimize sensitivity to the polarization fluctuation [23,24]. The vector shift and the field fluctuations are corrected as we interrogate two opposite spins of the atoms. After the clock interrogation, we ramp the lattice up to $300E_r$ and measure the excitation fraction with a standard shelving technique. The camera readout provides a high-resolution spatial distribution of the density and excitation fraction. With this information, we correct the density shift shot by shot [14], providing a robust rejection of systematics related to the atomic density fluctuation.

To establish the lattice, we seed the in-vacuum cavity with an injection-seeded diode laser (< 500 mW) to reach a lattice depth up to $300E_r$ with the waist w_0 of 260 μm. A volume Bragg grating with 50 GHz bandwidth and the optical cavity finesse of 1000 greatly suppress the broad spectral background of the diode laser [25]. With the lattice laser frequency locked to a cavity resonance, the cavity itself is stabilized to an absolute frequency-stabilized optical frequency comb. For lattice frequency modulation, we vary a comb-lock offset frequency so the cavity continuously follows the laser during the sample preparation before the last cooling stage. This scheme allows us to change the lattice frequency by ±200 MHz within 200 ms, suitable for interleaved self-comparison.

Rabi excitation of Wannier-Stark states.—Understanding atom-laser interaction at the shallow lattice depth is essential for the light shift evaluation. The tunneling rate between the lattice sites is exponentially sensitive to u. Hence, for small u, the extent of the delocalized atomic wave function can be larger than the clock laser wavelength [Fig. 1(b)], resulting in a breakdown of the Lamb-Dicke regime and a dramatic reduction of the clock drive Rabi frequency. We note that the long atom-light coherence is critically important here as it ensures a resolved sideband regime for spectroscopy. A time-domain Rabi oscillation signal is fit with a decayed sinusoidal curve to extract the Rabi frequency [19]. Relative Rabi frequencies of the carrier and three site-changing transitions (WS + i) are shown in Fig. 2 for the $n_z = 0$ and $n_z = 1$ motional states. Solid lines are numerically calculated Rabi frequencies fitted to the data with two fitting parameters: the cavity-transmitted light intensity conversion factor to lattice depth and an overall normalization factor for Rabi frequency. We calibrate the peak lattice depth U_0 based on this fit, and the uncertainty is $0.1(0.6)E_r$ at $U_0 = 0(300)E_r$.

The increased sensitivity of the Rabi frequency on the lattice depth is reflected in its radial variation. Consequently, coupling to the second order radial sidebands becomes more pronounced, especially for $|n_z = 1\rangle$. See Supplemental Material for the details [19].

Deviation from the stationary state.—At very low lattice depths ($\lesssim 6E_r$), stationary Wannier-Stark states may no longer be supported, as evidenced by the increasingly large effective tunneling rate in Fig. S8 of Supplemental Material [19]. We observe a deviation of the measured data from the lattice light shift model, with a rapid deterioration of the model fit if we include increasingly low lattice depth data [19].

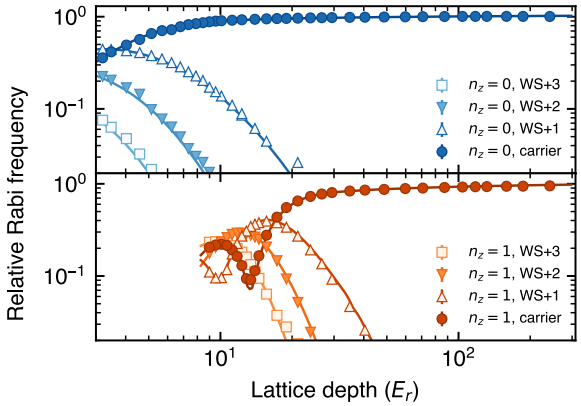

FIG. 2. Rabi frequency for the carrier and WS + i transitions. Measured Rabi frequencies are normalized to the maximum value. The upper (lower) panel shows WS + i transitions of $|n_z = 0\rangle$ ($|n_z = 1\rangle$). The error bars indicate 1 standard deviation from the fitting. Solid lines are theory calculations. The lattice depth U_0 is fit to these data for the calibration. As we reduce U_0, atoms are delocalized and their coupling to the clock laser drive is reduced significantly.

This deviation depends on the lattice depth U and is insensitive to δ_L. We vary other experimental conditions such as π-pulse duration, changing the initial state to $^3P_0$, and the bias field strength, with no effect on the deviation at the lowest trap depths. Therefore, we conclude that it is not from the lattice light shift. We compare two π-pulse durations that differ by factor 3 and observe no difference, suggesting the line pulling effect from the Bloch oscillation or the superposition of different WS states do not contribute to the deviation.

To add experimental evidence to the underlying mechanism of this deviation, we compare the clock frequency between the upward and downward propagation direction under otherwise the same condition [19]. We find that the frequency deviation from the model using the opposite clock laser propagation has the same magnitude and

TABLE I. Summary of the light shift characterization. We perform a single fit to the data including both Figs. 3 and 4 to extract the coefficients. For an operational condition [$u = 10(0.2)$, $\delta_L = 0(0.1)$ MHz, $n_z = 0(0.03)$], the uncertainty of the lattice light shift is 3.5×10^{-19}.

Quantity	Value
$\partial_\nu \tilde{\alpha}^{E1}/h$	$1.859(5) \times 10^{-11}$
ν^{E1} (MHz)	368 554 825.9(4)
$\tilde{\alpha}^{qm}/h$ (mHz)	−1.24(5)
$\tilde{\beta}/h$ (μHz)	−0.51(4)

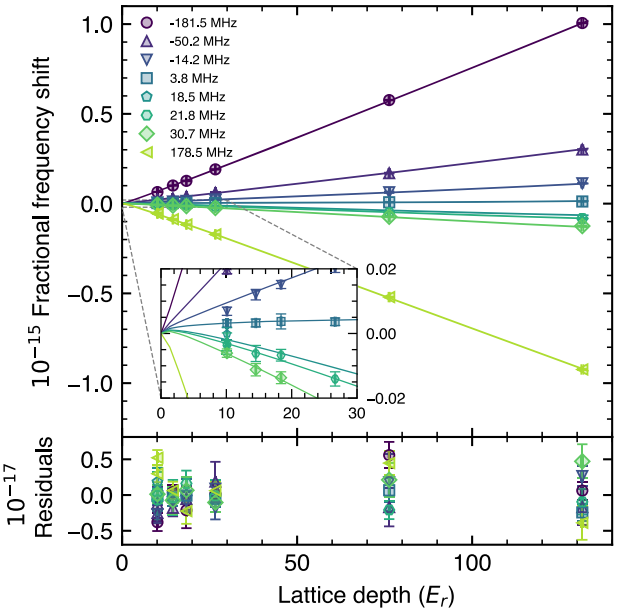

FIG. 3. Lattice depth (U_0) and detuning (δ_L) dependent light shift. Different markers represent different δ_L from the fit. For visualization, we offset the reference condition of each data point using the global fitting result. The inset (enlargement) emphasizes a nonlinearity near the zero depth. The solid lines fit the model Eq. (1). The fitting result is summarized in Table I. We excluded data for $< 8E_r$ (see text for the details). The error bars show the 1σ of statistical uncertainties. The shift uncertainty is calculated at $1/3$ total measurement time using a $1/\sqrt{\tau}$ fit to the overlapping Allan deviation, and the depth uncertainties are from the lattice depth calibration.

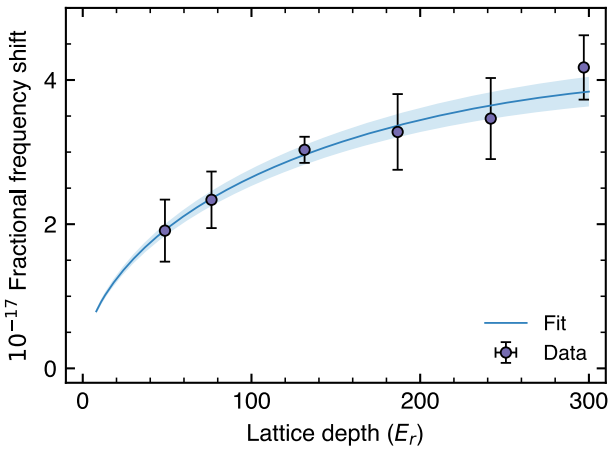

FIG. 4. Axial state dependent light shift, $\Delta\nu_{\mathrm{LS}}(u, \delta_L, n_z = 1) - \Delta\nu_{\mathrm{LS}}(u, \delta_L, n_z = 0)$, where $\delta_L < 1$ MHz. We plot n_z modulated part of the dataset with good sensitivity to the multipolar polarizability $\tilde{\alpha}^{qm}$. The solid line is fitting to the model Eq. (1) and the shades show 1σ deviation of $\tilde{\alpha}^{qm}$. Data points with $U_0 < 30E_r$ are excluded from the fit (see text for the details). The shift uncertainty is calculated at $1/3$ total measurement time using a $1/\sqrt{\tau}$ fit to the overlapping Allan deviation.

opposite sign. Based on these observations, we exclude data where $U_0 < 8E_r$ for (u, δ_L) modulation and $U_0 < 30E_r$ for n_z modulation from the fit.

Lattice light shift evaluation.—We explore Eq. (1) in a self-contained manner with all three control parameters (u, δ_L, n_z) and extract all the coefficients simultaneously. The results are summarized in Table I. The residual variance (reduced χ^2) of the fit is 1.3. The overall uncertainty includes inflation by the square root of the reduced χ^2 and other systematic uncertainties from T_r. For an operational condition [$u = 10(0.2)$, $\delta_L = 0(0.1)$ MHz, $n_z = 0(0.03)$], the uncertainty of the lattice light shift is 3.5×10^{-19}.

Figure 3 displays the light shift measurement investigating the dependence on u and δ_L. For this plot, only the carrier transition for $|n_z = 0\rangle$ is employed. By choosing the reference condition near the magic lattice depth ($10E_r$) where the atomic density effect is suppressed [1,14], we establish a reference frequency with minimal potential systematic effects.

Figure 4 shows n_z dependent light shift. For this part of the data, we keep the other control parameters (u, δ_L) the same. We determine $\tilde{\alpha}^{qm} = -1.24(5)$ mHz. This value is close to recent measurements in deep lattices [16,26]. A difference from Refs. [16,26] is that we use magnetic field insensitive spin states and microscopically determined n_z-dependent density shift coefficients (~20% difference between $n_z = 0$, 1) to suppress systematics [1,14]. While theory predictions still have disagreements [17,27–30], we became aware of a new theoretical calculation of $\tilde{\alpha}^{qm}$ [31] that is in agreement with experimental observations. The measured $\tilde{\beta}$ has a negligible contribution from the coupling of vector and tensor polarizability [24], and it agrees with the previous measurements [6,16,23,27,32].

Conclusion.—With precise control of the motional states in a Wannier-Stark optical lattice, we show that an important systematic effect, the lattice light shift, is measured and controlled at the 3.5×10^{-19} uncertainty. This result is unique in that the light shift model is tested for very shallow lattices. This is important for achieving high accuracy optical lattice clocks for the future definition of the SI second.

We thank D. Kedar and C. Kennedy for technical discussions and assistance. We thank A. Chu and W. McGrew for careful reading of the manuscript and useful comments. Funding support is provided by NSF QLCI OMA-2016244, DOE Center of Quantum System Accelerator, DARPA, NIST, and NSF Phys-1734006. K. K. was supported by the education and training program of the Quantum Information Research Support Center, funded through the National Research Foundation of Korea (NRF) by the Ministry of science and ICT (MSIT) of the Korean government (No. 2021M3H3A103657313).

[1] T. Bothwell, C. J. Kennedy, A. Aeppli, D. Kedar, J. M. Robinson, E. Oelker, A. Staron, and J. Ye, Resolving the gravitational redshift across a millimetre-scale atomic sample, Nature (London) **602**, 420 (2022).

[2] X. Zheng, J. Dolde, V. Lochab, B. N. Merriman, H. Li, and S. Kolkowitz, Differential clock comparisons with a multiplexed optical lattice clock, Nature (London) **602**, 425 (2022).

[3] A. D. Ludlow, M. M. Boyd, J. Ye, E. Peik, and P. O. Schmidt, Optical atomic clocks, Rev. Mod. Phys. **87**, 637 (2015).

[4] T. Bothwell, D. Kedar, E. Oelker, J. M. Robinson, S. L. Bromley, W. L. Tew, J. Ye, and C. J. Kennedy, JILA SrI optical lattice clock with uncertainty of 2.0×10^{-18}, Metrologia **56**, 065004 (2019).

[5] W. F. McGrew, X. Zhang, R. J. Fasano, S. A. Schäffer, K. Beloy, D. Nicolodi, R. C. Brown, N. Hinkley, G. Milani, M. Schioppo, T. H. Yoon, and A. D. Ludlow, Atomic clock performance enabling geodesy below the centimetre level, Nature (London) **564**, 87 (2018).

[6] R. Le Targat, L. Lorini, Y. Le Coq, M. Zawada, J. Guéna, M. Abgrall, M. Gurov, P. Rosenbusch, D. G. Rovera, B. Nagórny, R. Gartman, P. G. Westergaard, M. E. Tobar, M. Lours, G. Santarelli, A. Clairon, S. Bize, P. Laurent, P. Lemonde, and J. Lodewyck, Experimental realization of an optical second with strontium lattice clocks, Nat. Commun. **4**, 2109 (2013).

[7] K. Beloy *et al.* (Boulder Atomic Clock Optical Network (BACON) Collaboration), Frequency ratio measurements at 18-digit accuracy using an optical clock network, Nature (London) **591**, 564 (2021).

[8] R. Hobson, W. Bowden, A. Vianello, A. Silva, C. F. A. Baynham, H. S. Margolis, P. E. G. Baird, P. Gill, and I. R. Hill, A strontium optical lattice clock with 1×10^{-17} uncertainty and measurement of its absolute frequency, Metrologia **57**, 065026 (2020).

[9] N. Nemitz, T. Ohkubo, M. Takamoto, I. Ushijima, M. Das, N. Ohmae, and H. Katori, Frequency ratio of Yb and Sr clocks with 5×10^{-17} uncertainty at 150 seconds averaging time, Nat. Photonics **10**, 258 (2016).

[10] I. Ushijima, M. Takamoto, M. Das, T. Ohkubo, and H. Katori, Cryogenic optical lattice clocks, Nat. Photonics **9**, 185 (2015).

[11] R. Schwarz, S. Dörscher, A. Al-Masoudi, E. Benkler, T. Legero, U. Sterr, S. Weyers, J. Rahm, B. Lipphardt, and C. Lisdat, Long term measurement of the ^{87}Sr clock frequency at the limit of primary Cs clocks, Phys. Rev. Res. **2**, 033242 (2020).

[12] H. Kim, M.-S. Heo, C. Y. Park, D.-H. Yu, and W.-K. Lee, Absolute frequency measurement of the ^{171}Yb optical lattice clock at KRISS using TAI for over a year, Metrologia **58**, 055007 (2021).

[13] P. Lemonde and P. Wolf, Optical lattice clock with atoms confined in a shallow trap, Phys. Rev. A **72**, 033409 (2005).

[14] A. Aeppli, A. Chu, T. Bothwell, C. J. Kennedy, D. Kedar, P. He, A. M. Rey, and Jun Ye, Hamiltonian engineering of spin-orbit-coupled fermions in a Wannier-Stark optical lattice clock, Sci. Adv. **8**, eadc9242 (2022).

[15] S. Blatt, J. W. Thomsen, G. K. Campbell, A. D. Ludlow, M. D. Swallows, M. J. Martin, M. M. Boyd, and J. Ye, Rabi spectroscopy and excitation inhomogeneity in a one-dimensional optical lattice clock, Phys. Rev. A **80**, 052703 (2009).

[16] I. Ushijima, M. Takamoto, and H. Katori, Operational Magic Intensity for Sr Optical Lattice Clocks, Phys. Rev. Lett. **121**, 263202 (2018).

[17] H. Katori, V. D. Ovsiannikov, S. I. Marmo, and V. G. Palchikov, Strategies for reducing the light shift in atomic clocks, Phys. Rev. A **91**, 052503 (2015).

[18] K. Beloy, W. F. McGrew, X. Zhang, D. Nicolodi, R. J. Fasano, Y. S. Hassan, R. C. Brown, and A. D. Ludlow, Modeling motional energy spectra and lattice light shifts in optical lattice clocks, Phys. Rev. A **101**, 053416 (2020).

[19] See Supplemental Material at http://link.aps.org/supplemental/10.1103/PhysRevLett.130.113203 for more information.

[20] E. Oelker, R. B. Hutson, C. J. Kennedy, L. Sonderhouse, T. Bothwell, A. Goban, D. Kedar, C. Sanner, J. M. Robinson, G. E. Marti, D. G. Matei, T. Legero, M. Giunta, R. Holzwarth, F. Riehle, U. Sterr, and J. Ye, Demonstration of 4.8×10^{-17} stability at 1 s for two independent optical clocks, Nat. Photonics **13**, 714 (2019).

[21] D. G. Matei, T. Legero, S. Häfner, C. Grebing, R. Weyrich, W. Zhang, L. Sonderhouse, J. M. Robinson, J. Ye, F. Riehle, and U. Sterr, 1.5 μm Lasers with Sub-10 mHz Linewidth, Phys. Rev. Lett. **118**, 263202 (2017).

[22] T. L. Nicholson, M. J. Martin, J. R. Williams, B. J. Bloom, M. Bishof, M. D. Swallows, S. L. Campbell, and J. Ye, Comparison of Two Independent Sr Optical Clocks with 1×10^{-17} Stability at 10^3 s, Phys. Rev. Lett. **109**, 230801 (2012).

[23] P. G. Westergaard, J. Lodewyck, L. Lorini, A. Lecallier, E. A. Burt, M. Zawada, J. Millo, and P. Lemonde, Lattice-Induced Frequency Shifts in Sr Optical Lattice Clocks at the 10^{-17} Level, Phys. Rev. Lett. **106**, 210801 (2011).

[24] C. Shi, J.-L. Robyr, U. Eismann, M. Zawada, L. Lorini, R. Le Targat, and J. Lodewyck, Polarizabilities of the ^{87}Sr clock transition, Phys. Rev. A **92**, 012516 (2015).

[25] R. Fasano, Y. Chen, W. McGrew, W. Brand, R. Fox, and A. Ludlow, Characterization and Suppression of Background Light Shifts in an Optical Lattice Clock, Phys. Rev. Appl. **15**, 044016 (2021).

[26] S. Dörscher, J. Klose, S. Maratha Palli, and Ch. Lisdat, Experimental determination of the $E2$-$M1$ polarizability of the strontium clock transition, Phys. Rev. Res. **5**, L012013 (2023).

[27] S. G. Porsev, M. S. Safronova, U. I. Safronova, and M. G. Kozlov, Multipolar Polarizabilities and Hyperpolarizabilities in the Sr Optical Lattice Clock, Phys. Rev. Lett. **120**, 063204 (2018).

[28] F.-F. Wu, Y.-B. Tang, T.-Y. Shi, and L.-Y. Tang, Dynamic multipolar polarizabilities and hyperpolarizabilities of the Sr lattice clock, Phys. Rev. A **100**, 042514 (2019).

[29] V. D. Ovsiannikov, S. I. Marmo, V. G. Palchikov, and H. Katori, Higher-order effects on the precision of clocks of neutral atoms in optical lattices, Phys. Rev. A **93**, 043420 (2016).

[30] V. D. Ovsiannikov, V. G. Pal'chikov, A. V. Taichenachev, V. I. Yudin, and H. Katori, Multipole, nonlinear, and

anharmonic uncertainties of clocks of Sr atoms in an optical lattice, Phys. Rev. A **88**, 013405 (2013).

[31] F.-F. Wu, T.-Y. Shi, and L.-Y. Tang, Contributions of negative-energy states to the E2-M1 polarizability of the Sr clock, arXiv:2301.06740.

[32] T. Nicholson, S. Campbell, R. Hutson, G. Marti, B. Bloom, R. McNally, W. Zhang, M. Barrett, M. Safronova, G. Strouse, W. Tew, and J. Ye, Systematic evaluation of an atomic clock at 2×10^{-18} total uncertainty, Nat. Commun. **6**, 6896 (2015).